PROCEEDINGS, 41st Workshop on Geothermal Reservoir Engineering
Stanford University, Stanford, California, February 22-24, 2016
SGP-TR-209

Propagation of Velocity Model Errors in Earthquake Absolute Locations: Application to the Rittershoffen Geothermal Field

Emmanuel GAUCHER[1], Xavier KINNAERT[1-2], Ulrich ACHAUER[2] and Thomas KOHL[1]

[1]KIT, Institute of Applied Geosciences, Division of Geothermal Research, Adenauerring 20b, D-76131 Karlsruhe, Germany

[2]EOST-IPGS UMR7516, 5 rue René Descartes, F-67000 Strasbourg, France

Email: emmanuel.gaucher@kit.edu

Keywords: seismic monitoring, network design, velocity model, location uncertainties, location inaccuracies, calibration

ABSTRACT

Hypocenter location of earthquakes is one of the most important sources of information to understand the physical processes at the origin of earthquakes, to describe the subsurface and to quantify earthquake seismic hazard. This characteristic is necessary to compute several other attributes of the seismic source, e.g. origin time, seismic moment, focal mechanism, which will complete the earthquake catalogue. However, location errors exist and need to be properly quantified because with the earthquake hypocenter they determine the meaningful scale of investigation.

We analyze for the Rittershoffen geothermal field (Upper Rhine Graben, France) the effect of velocity model errors on the determination of earthquake absolute locations. To do so, we first generate synthetic earthquakes in the geothermal reservoir and calculate in a 3D fault model the associated travel times on several seismic networks. Then, we relocate the events using a non-linear absolute location procedure, however in a reference 1D velocity model, as it is typically assumed for initial data processing. Thereby, we introduce velocity model errors between the synthetic and the relocation phases. The synthetic events are distributed in a volume where seismicity was induced during stimulations of the geothermal well GRT1. They range approximately between 1 and 4 km depth within a radius of 1.5 km around the well-head. The lay-out of the seismic network monitoring these operations is used as well as two other ones that are representative of the network densification over time.

The results show that the reference 1D velocity model, despite built from well log data, is not a good representative of a more realistic 3D model including a fault and its associated block shift. The seismic network coverage and the velocity model control the amplitude and orientation of the induced relocation uncertainties and inaccuracies in the zone of interest, which are neither constant nor aleatoric. Although a denser network with better coverage clearly decreases location uncertainties, location inaccuracies can still increase and be much larger than the uncertainties. This emphasizes the very different behavior and physical meaning between both quantities, which should not be confused. The induced location inaccuracies may be such that the positioning and orientation of features delineated by seismicity are strongly distorted and difficult to correctly interpret, even in the case of a very dense seismic network. However, we show that a calibration shot can remove most of these effects.

1. INTRODUCTION

In applications such as geothermal energy production, oil and gas production, underground storage or mining, it is worth deploying seismic networks, both for seismic hazard mitigation and reservoir description. In geothermal contexts, the understanding of the physical processes at the origin of the induced seismicity greatly increased with the observation and analysis of this phenomena (Cornet, Bérard and Bourouis 2007; Lengliné *et al.* 2014; Zang *et al.* 2014; Gaucher *et al.* 2015b), as well as the development of forecasting approaches (Gaucher *et al.* 2015a). Besides, induced seismicity always contributes to the identification of faults in the reservoir (Sausse *et al.* 2010; Kraft and Deichmann 2014; Edwards *et al.* 2015; Frietsch, Groos and Ritter 2015). In many cases, this allowed optimizing well trajectories, and sometimes to evaluate the field economic performances (e.g. Held *et al.* 2014). Therefore, within such industrial contexts, earthquake hypocenters and their associated errors can have a major impact on the field development and economic consequences.

The earthquake location error may be defined as the combination of two quantities: the location inaccuracy and the location imprecision. The latter is taken equivalent to the *a posteriori* location uncertainties resulting from the propagation in the inverse location problem of the *a priori* uncertainty (e.g. Tarantola 2005). Typically, *a priori* picking uncertainties of seismic waves are integrated in the inverse problem and lead to *a posteriori* location uncertainties, which are part of the location result. On the contrary, the location inaccuracy is defined as the wrong positioning of the hypocenter due to all effects that have been overlooked in the inverse problem. These simplifications of the reality introduce bias in the computation of the earthquake location. The use of a seismic velocity model not representative of the effective propagation medium would, most of the time, lead to earthquake location inaccuracies (Pavlis 1986; Bardainne and Gaucher 2010; Husen, Kissling and Deschwanden 2013), except in the approach of Gesret *et al.* (2015) for example. Although earthquake hypocenters may be provided with uncertainties, they are rarely given with inaccuracies. Yet, to avoid misleading seismicity interpretation, it is crucial to know the latter because they may be much larger than the former and they often behave differently. This issue motivated the present work and its application to the deep geothermal field of Rittershoffen (France). This enhanced geothermal system (EGS) is located in the Upper Rhine Graben (URG) and the seismicity induced by its development is being

analyzed (Maurer *et al.* 2015). Rittershoffen is also surrounded by existing EGS (e.g. Soultz-sous-Forêts (France), Insheim (Germany)) or potential fields under exploration, which could benefit from the general conclusions of this study.

In this work, we focus on uncertainties and inaccuracies of absolute location of earthquakes in underground reservoirs. Therefore, neither relative location algorithms of earthquakes based on double-differences (e.g. Waldhauser and Ellsworth, 2000) or master-slave events (e.g. Fréchet, 1985, Poupinet *et al.*, 1985), nor location techniques based on waveform stacking and migration from dense array recordings (Kao and Shan, 2004, Gharti *et al.*, 2010, Drew *et al.*, 2013, Grigoli *et al.*, 2013) are considered.

After presenting the methodology to quantify the hypocenter location inaccuracies and uncertainties, we present the Rittershoffen geothermal field to understand the context and the input parameters used in this study. Then, we apply realistic scenarios, both regarding the seismic network design and the velocity model error, to quantify their impact on the location errors. We focus on the use of a 1D velocity model in place of a 3D fault-model and on the value added by a calibration shot. Other realistic scenarios are covered by Kinnaert *et al.* (in revision).

2. METHODOLOGY

To quantify earthquake location inaccuracies and uncertainties, a multi-step approach is applied. First, synthetic earthquake hypocenters are defined and, in a given velocity model, forward modeling of the P- and S-wave travel times to the seismic stations of a network are computed. For this step, we use the numerical code of Podvin and Lecomte (1991), which is applicable in any type of seismic velocity model. A 3D fault model will be tested (see subsection 3.3). The sources are positioned in the reservoir, where they are expected to occur. Then, the synthetic travel times will be considered as the arrival times observed at each station of the network. Second, the earthquakes are relocated using the simulated times but in a velocity model different from the initial one. The relocation velocity model will be kept constant throughout the study and is defined by a series of horizontal layers of constant P- and S-wave velocities (Vp, Vs) but varying Vp/Vs ratio (see subsection 3.3). Such a 1D velocity model is taken because it is still representative of velocity models used for local seismicity processing at the scale of underground reservoirs. This is precisely the effects of such simplifications that we want to quantify. To relocate the synthetic events, the numerical code NonLinLoc (NLL) developed by Lomax *et al.* (2000) is used. This code keeps the intrinsic nonlinearity of the location problem and is suitable for locating earthquakes at a reservoir scale using a grid-search. The absolute location method proposed by Wittlinger, Herquel and Nakache (1993) and implemented in NLL will be used. It computes the probability density function (PDF) of an earthquake hypocenter at a location $\boldsymbol{X}$, from the Bayesian and least-square formalism presented by Tarantola and Valette (1982):

$$\mathrm{PDF}(\boldsymbol{X}) = K \cdot \exp\left\{-\frac{1}{2}\left(\left[\widetilde{\boldsymbol{T}}_{Obs} - \widetilde{\boldsymbol{T}}_{Calc}(\boldsymbol{X})\right]^{t} \cdot \boldsymbol{C}^{-1} \cdot \left[\widetilde{\boldsymbol{T}}_{Obs} - \widetilde{\boldsymbol{T}}_{Calc}(\boldsymbol{X})\right]\right)\right\} \quad (1)$$

with K a normalizing constant, $\widetilde{\boldsymbol{T}}_{Obs}$ the vector of the seismic arrival times observed at the seismic stations minus their weighted mean, $\widetilde{\boldsymbol{T}}_{Calc}$ the vector of the computed travel times minus their weighted mean, and $\boldsymbol{C}$ the *a priori* covariance matrix. The computation of the theoretical travel times ($\widetilde{\boldsymbol{T}}_{Calc}$) is done also using the Podvin and Lecomte (1991) numerical code (but in the 1D model). The picking uncertainties or standard deviations of the observed arrivals times ($\boldsymbol{T}_{Obs}$) will form the *a priori* covariance matrix $\boldsymbol{C}$ (see subsection 4.1 for details). The earthquake hypocenter is located where the PDF is the highest, which corresponds to the smallest misfit (right term in brackets in Eq. 1). Since the PDF is estimated everywhere in the location zone, the true *a posteriori* earthquake location uncertainty is available in the 3D space.

Once the synthetic earthquake relocation is obtained, it is compared to the initial location to quantify the location error. The spatial distance separating the original hypocenter with the relocated one gives the location inaccuracy. The 68.3% confidence domain around the event relocation is associated with the location uncertainty. Assuming a Gaussian distribution of the PDF around the relocated event, principal component analysis of the confidence ellipsoid gives the three orientations and lengths of the uncertainty orthogonal axes. In the following, the location uncertainty will be quantified by the half-length of the largest confidence ellipsoid axis and, therefore, the location should be understood within ± the uncertainty length.

3. THE RITTERSHOFFEN GEOTHERMAL FIELD

3.1 Field Context

The deep geothermal field of Rittershoffen (Alsace, France) is located 7 km to the East of the Soultz-sous-Forêts geothermal field (Figure 1). Like the latter, it is in the western part of the Upper Rhine Graben (URG), which exhibits many positive heat anomalies (Baillieux *et al.* 2013) due to complex subsurface structures. Several graben and horst structures are delimited by synthetic and antithetic faults, predominantly striking N-S to NNE-SSW. The granitic basement is highly fractured and faulted and shows alteration below its boundary with the overlying sediments (Genter 1989). These geological characteristics favor the exploitation of this renewable energy resource in the area (e.g. Landau, Insheim, Bruchsal, all in Germany) and the exploration activity (Meixner *et al.* 2016).

The ECOGI joint venture (Electricité de Strasbourg group, Roquette Frères and Caisse des Dépôts et de Consignation) is in charge of the development and exploitation of the Rittershoffen field which is one of the very few currently under development in Europe. The objective is to produce, mid-2016, 24 MWth (170 °C, 70 L/s) to a bio-refinery plant located 15 km away. The location was chosen because it sits over one of the largest thermal gradient observed in the URG, leading to temperatures close to 165°C at 1800 m depth (Baujard *et al.* 2014). Unlike the Soultz-sous-Forêts geothermal field, but like the Landau and the Insheim ones, the Triassic sandstone and the underlying Paleozoic granite constitute the exploited reservoir formations. Between 2012 and 2014, the drillings and development of the underground reservoir were carried out. Both wells of the doublet are drilled to 2500 m, 200 m below the Buntsandstein – granite interface. To increase the chance to access permeable zones, the geothermal wells target a normal fault which

delimits two geological blocks (Figure 1). This fault, approximately oriented N-S with a dip of 60°W, accounts for ~200 m vertical shift.

In 2013, successful stimulations were performed in the first well, GRT1, to enhance its connectivity with the reservoir (Baujard *et al.* 2014). These operations were applied in two sequences, respectively in April 2013 and in June 2013; both induced seismicity (Maurer *et al.* 2015). Many hundreds of events were recorded by a surface seismic network, detected and located, all with local magnitude smaller than M_L=1.6. The seismicity concentrates in the SW of GRT1 and between 1.5 and 3.5 km depth. The seismic cloud is roughly oriented N-S to NNE-SSW and is approximately 2 km long, 1 km wide and 2 km high. The second well, GRT2, was not stimulated because sufficient natural artesian fluid could be produced from it.

According to the distribution of the induced seismicity, we will generally distribute the synthetic earthquake hypocenters in a cube of approximately 4 km side centered on the GRT1 open-hole mid-depth (small grey rectangle in Figure 2). The sources will be regularly spaced either in the 3D volume, or on several planes included in the volume. The detailed positions will be presented in each of the examined scenarios.

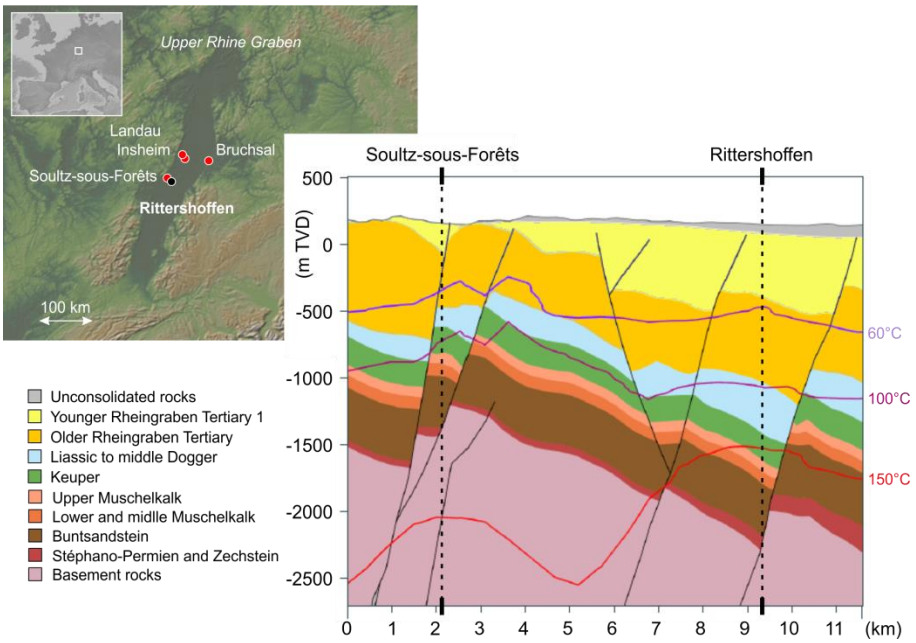

Figure 1: Top left: general view of the Upper Rhine Graben and of the deep geothermal fields close to Rittershoffen (black circle). Bottom right: vertical cross-section of the geological structure between the Soultz-sous-Forêts and the Rittershoffen fields.

3.2 Seismic Monitoring Network

Prior to and during the geothermal reservoir development, the area was monitored by a seismic network which became denser over time (Gaucher *et al.* 2013). This study uses three network lay-outs. First of all, the network monitoring the chemical and hydraulic stimulations of the well GRT1 (June 2013) is used as a reference for the location error analysis because it recorded one of the most seismogenic field operations. It is made of 17 surface stations: 12 with a three-component seismometer and the remaining with a vertical seismometer. Among these 17 stations, the furthest two (GUNS and LAMP, both single-components) are not used because the low signal to noise ratio of the induced seismicity prevented from any P- or S-wave picking (N. Cuenot, pers. comm., 2015). As shown in Figure 2, this network, called Net15, covers only the northern part of GRT1, and the associated effect on the earthquake location errors will be shown. Permitting issues prevented from deploying seismic stations in the southern part of GRT1 before its stimulation. However, this could be done before drilling the second well. Accordingly, we also discuss the effect of adding one surface station in the forest, E3316 (three-components); this will form the so-called network Net16 (Figure 2). Finally, before drilling the GRT2 well, 25 surface stations (three-components) were deployed to finalize the dense network (Figure 2). The lay-out associated with these 41 usable stations in total is the third network we consider in the study and is called Net41. Compared to Net15, it is now centered on the well pad and the stations are homogeneously distributed, almost every 1.5 km, over an area of 5 km radius.

3.3 Seismic Velocity Models

In this study, two velocity models are considered. As a reference, we take the 1D velocity model that was used by Maurer *et al.* (2015) to process the induced seismicity. Therefore, we will always relocate the synthetic sources in this model. It was created from several logs ran in the GRT1 well (geological, compression- and shear-velocity and zero-offset VSP logs). For each major stratigraphic layer

identified in the well, a constant Vp was calculated using the VSP data. The compression- and shear-velocity log was used to compute the corresponding average Vp/Vs ratio. Figure 3 shows the P- and S-wave velocity profiles at Rittershoffen. Vp ranges between 1320 m/s and 5815 m/s from surface to the granite, and Vs between 620 m/s and 3275 m/s. Two large velocity contrasts are observed at the top of the Lias layer (1365 m) and at the top of the granite (2200 m), as well as three low-velocity layers between 1025 – 1300 m, 1630 – 2000 m and 2100 – 2200 m depth. Note that the Vp/Vs ratio varies between layers, from 1.68 to 2.12.

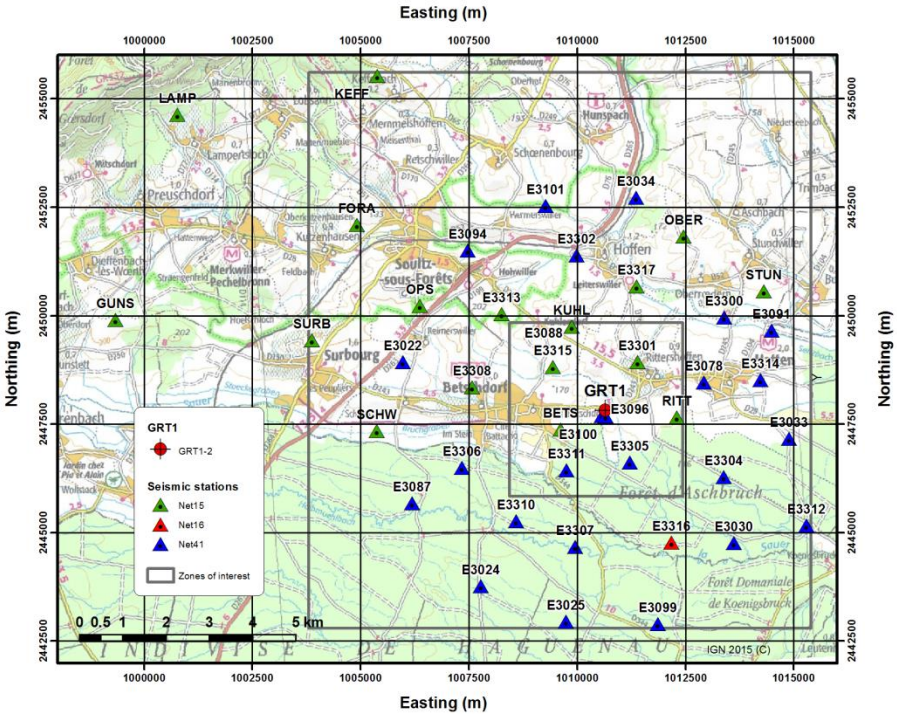

Figure 2: Map of the seismic networks deployed at the Rittershoffen geothermal field. The Net15 seismic network (green triangles) monitored the chemical and hydraulic stimulation of the GRT1 well. The Net16 seismic network consists of the Net15 with the additional station E3316 (red triangle). The Net41 seismic network, which was monitoring before drilling of the GRT2 well, corresponds to the Net16 with the additional stations displayed as blue triangles. Also shown are the GRT1 wellhead (red crossed circle), the velocity model zone used in this study (largest grey rectangle) and the area in which the seismic sources are simulated (smallest grey rectangle). All coordinates are in Lambert II extended system.

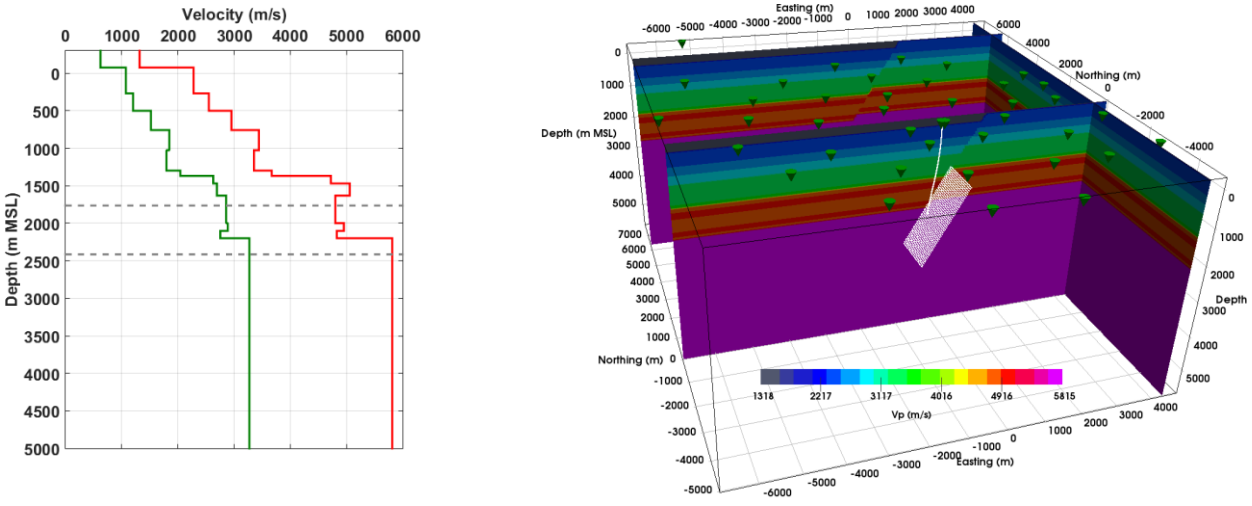

Figure 3: Rittershoffen velocity models. Left: reference 1D profile for the P-wave (red curve) and the S-wave (green curve) velocities with indication of the injection depth range in the well GRT1 (horizontal dashed lines). Right: view of the 3D fault model of the P-wave velocity (color scale) with indication of the GRT1 well trajectory (white curve) and of synthetic sources distributed on the fault around the well (white dots) (see subsection 4.2 for details).

In the specific geological context of Rittershoffen, the normal fault sitting below the site plays an important role in the underground reservoir development (Figure 1). This fault was expected to be more permeable than the surrounding matrix thus a good fluid pathway. Hence, both wells of the doublet were designed to cross the fault and, after drilling and testing, the expectation was confirmed. This major N-S fault dipping 60°W separates in two blocks the sedimentary formations and, at least, the shallower part of the crystalline rock. It crosses the GRT1 well at 2200 m and is associated with a vertical displacement of about 200 m which shifts up the eastern block relative to the western one. It is therefore realistic to construct a 3D model including the fault and the associated velocity changes: the reference 1D-velocity profile is kept for the western block but is shifted 200 m upward (along the fault) for the eastern block (Figure 3).

In subsection 4.2, we investigate the location errors caused by the use of the reference 1D velocity model in place of the 3D fault model.

In the NLL location numerical code, the 1D and the 3D velocity models are discretized on a 10-m and 20-m mesh size in the East, North and depth directions respectively.

4. RESULTS AND DISCUSSIONS

In this section, we investigate the location uncertainties and inaccuracies, which are induced at Rittershoffen by using the 1D velocity model to relocate the synthetic earthquakes instead of the 3D fault model, which was used during the modelling step. We also examine the value added by a calibration shot. Other scenarios associated with velocity model errors are analyzed by Kinnaert *et al.* (in revision). The three monitoring networks described above will be considered. For clarity purpose, we present the geographical results relative to the GRT1 wellhead (1010653.18 m East, 2447831.75 m North, Lambert II extended). Unless specified, the depth is a true vertical depth from mean-sea-level given in meter.

4.1 Location Uncertainties Caused by Picking Uncertainty

Before focusing on the location inaccuracies, we first look at the *a posteriori* location uncertainties resulting from the *a priori* picking uncertainties, in the reference 1D velocity model.

The manual processing of the seismicity induced at Rittershoffen allowed us defining the picking uncertainties of the P- and S-wave arrivals. It was noticed that no picking uncertainty difference exists between the P- and the S-wave arrival times (N. Cuenot, pers. comm., 2015). For all stations within a radius of 4 km around GRT1 (see Figure 2), the P- and S-picking uncertainties were set to ±20 ms, except for the stations E3096, E3100 and E3078 which were noisier and where the uncertainties were set to ±50 ms. For all remaining stations (i.e. outer-rim of the radial network and the western stations), the uncertainties were taken equal to ±50 ms. These values populate the matrix $\boldsymbol{C}$ of Eq. 1 and will be applied in the rest of the study. For all networks (Net15, Net16 and Net41), the P- and S-wave arrivals are used to relocate the synthetic sources for any three-component sensor whereas only the P-wave arrivals are used for vertical sensors. For this analysis, the synthetic sources were placed every 200 m in the 3D cube centered at the bottom of the GRT1 well.

Figure 4 shows sections of the location uncertainties in the reference 1D model and for the 3 different networks. As mentioned in section 2, the uncertainty corresponds to the length of the largest axis of the 68.3% confidence ellipsoid and, therefore, the location should be understood within ± the given values. From the horizontal sections made at the bottom of the GRT1 well, we observe that the uncertainties vary in the location zone for the Net15 and Net16 but are almost constant for the Net41. The effect is clearly due to the network coverage. Since Net15 is mainly located at the NW of the zone of interest, the location uncertainties are larger at the S-E side of the location zone. This effect is attenuated by the addition of the station in the forest (Net16) and almost disappears when the network becomes homogeneous around the target (Net41). Such a horizontal variability is kept over depth. The uncertainties are also varying and increasing generally with depth, for all considered networks. The large uncertainty variations occur at the interfaces with large velocity contrasts (e.g. at ~1400 m and 2200 m), but within a velocity layer, the uncertainties tend to remain relatively constant with depth (for example in the granite). Again, with the increasing network coverage, the lateral variation of the location uncertainties is decreasing. Regarding the amplitude of the uncertainties, they range between ±30 m and ±245 m for Net15, between ±30 m and ±235 m for Net16 and from ±20 m and ±115 m for Net41. So, the addition of stations (with improved coverage) both decreases the location uncertainties, as expected, but also the range and discrepancy over the location zone. These results show that the location uncertainties of the seismicity induced during the GRT1 well (i.e. with Net15) is of the order of ±150 m, which corresponds to ~6% of the distance to the surface.

In this case, where the velocity model did not change between the synthetic step and the relocation step, there is no location inaccuracy.

4.2 Location Errors Caused by Using the 1D Model Instead of the 3D Fault Model

Here, we investigate the effect of locating earthquakes in the 1D velocity model although the true Earth is represented by the 3D fault model (see subsection 3.3). To do so, four squared planes of 2400 m side length, with synthetic earthquakes distributed every 50 m, and centered on the injection mid-depth are created. Two of them are vertical, striking N-S and striking E-W, another one is horizontal, and the last plane corresponds to the fault plane. Figure 3 (right) shows the location of the sources on the fault plane.

Figure 5 shows, for the three networks, the four initial earthquake planes and the corresponding four surfaces on which the earthquakes are relocated.

One can first note that, whatever the seismic network considered, large location inaccuracies are induced by using the 1D velocity model instead of the 3D fault model. The earthquakes have the main tendency to be systematically relocated eastward from their initial position. This observation is consistent with the results obtained by Pavlis (1986) for a comparable simulation of a two-block velocity

model in the Morgan Hill area (California). Since the location inaccuracies are varying in direction and in amplitude, the initial planes of sources become curved surfaces.

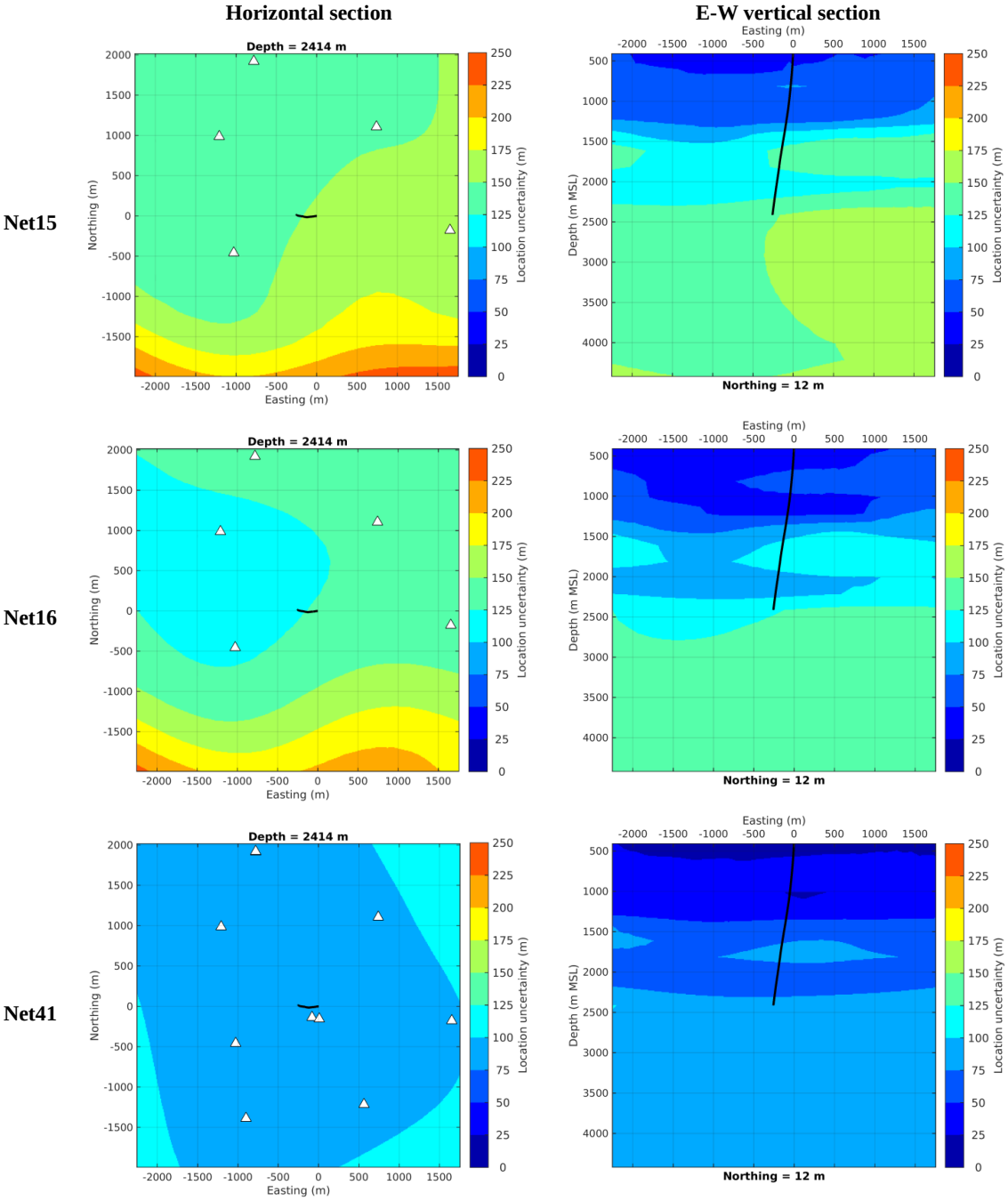

Figure 4: Location uncertainties in 1D velocity model. Horizontal sections at 2414 m (left column) and E-W vertical sections at 12 m Northing (right column), for the Net15 (top row), Net16 (middle row) and Net41 (bottom row) networks. The stations above the location zone are displayed (white triangles) as well as the GRT1 well trajectory (black curve).

The sources initially located on the fault are systematically shifted eastward and deeper. In addition, for Net15 and its relatively poor coverage compared to Net16 and Net41, the sources located north of GRT1 well move slightly southward but northward for those located south of GRT1 well. The median horizontal shift, dominated by the eastern shift, ranges between 300 and 350 m for Net15 and between 360 and 450 m for Net41. The median depth shift ranges, for Net15, between 55 and 200 m for the deepest and shallowest sources respectively but between 125 and 260 m for the Net41. Despite these spatial inaccuracies, the average azimuth and dip of the

relocated source surface are similar to the initial source plane. Nevertheless, a more complex transformation is observed for the three other planes of synthetic sources which are not parallel to the fault, but the complexity decreases with increasing network coverage. In these cases, the initial planes are deformed in a continuous manner which depends on the initial source locations.

For the horizontal plane crossing the GRT1 injection mid-depth, the eastern shift increases with increasing sources longitude and the initial southward shift becomes a northward shift. This behavior is observed for the three networks except the N-S shifts which disappear with increasing network coverage. The eastern shift is always dominating and the median horizontal location inaccuracies vary from 250 to 350 m from the western to the eastern side of the plane for Net15 and from 310 to 440 m for Net41. Still from West to East, the depth difference between the relocated and the initial sources decreases from 230 to -30 m for Net15 and from 310 to -10 m for Net41, which means that, although the sources are relocated deeper than expected on the western side of the plane, they are shallower on the eastern side.

The sources of the E-W vertical plane are relocated eastward from their original position with increasing shifts from the upper side of the original plane to the lower one. With Net15, an original southward shift from the western side of the E-W plane becomes a northward shift at the eastern side of the plane, but this behavior is not observed any longer once the network coverage is good, i.e. with Net41. The median of the horizontal inaccuracies ranges between 250 and 320 m with Net15 but between 310 and 430 m with Net41. With regards to the depth, the events at the upper-western part of the plane are relocated deeper with the largest vertical shift but those at the lower-eastern part are found shallower with the smallest vertical shift. The median depth inaccuracies range from -90 to 240 m with Net15 and from 0 to 300 m with Net41.

At last, the N-S vertical plane moves eastward with a larger offset as depth increases. A southward-down shift from the upper-northern corner of the N-S plane becomes a northward-up shift at the lower-southern corner of the plane. The median of the horizontal inaccuracies increases regularly with depth from 200 m in the sediments to 400 m in the granite with Net15 but from 240 to 470 m with Net41. Regarding the vertical inaccuracies, they vary between -50 m (shallower) in the bedrock to 230 m in the sediments for Net15 but from 0 to 310 m with Net41.

These results show that the addition of one or more stations to the smallest network Net15 does not improve the location accuracy, on the contrary. This is because the improvement of the network coverage over the location zone (with Net16 and Net41) increases the number of observations in contradiction with the assumed 1D velocity model. In other words, any new seismic ray between one event and one station traveling through the 3D fault model brings more inconsistency in the – least-square – location inverse problem.

The location inaccuracies have consequences on the interpretation of planar features delineated by earthquake hypocenters. First, locating in the 1D velocity model instead of the 3D fault model leads to systematically relocate the earthquakes eastward from their initial position, from several hundreds of meters. As a consequence, any plane defined by earthquakes is shifted to the East. Besides, since western and eastern earthquakes are shifted differently in depth, original source planes will dip more to the west after relocation. Finally, an initial vertical plane of sources will be rotated counter-clockwise after relocation with the low coverage network Net15. This effect, however, disappears with the coverage improvement of Net 16 and mainly Net41. This is due to the fact that Net41 covers almost homogeneously the reservoir and that the E-W vertical section is a symmetry plane for the velocity model. Such symmetry in the system is at the origin of the relocation by Net41 of the sources of the E-W vertical plane still on that plane. All these plane rotations and shifts will generally cumulate but the better coverage of the location zone by Net41 decreases the local distortion and the bending of initial source planes (although the inaccuracies are still the largest with this network).

The uncertainties associated with the relocated sources are also presented in Figure 5 with the color scale visible on the surfaces. As observed, for all networks, the uncertainty amplitudes are of the order of those calculated in the unchanged 1D velocity model (see previous subsection): up to 250 m with Net15, 225 m with Net16 and 100 m with Net41. They decrease with the increasing number of stations in the network. Moreover, the depth distribution of the uncertainties is still correlated with the velocity contrasts in the 1D model, especially on the western side of the fault; on the eastern side, there is distortion of the uncertainties due to velocity inconsistencies between the 3D fault model and the 1D model.

When considering both the location uncertainties and inaccuracies, we clearly see that the higher the number of stations in the network the smaller will be the former but the larger will be the latter. In addition, the inaccuracies are always larger than the uncertainties. So, these two quantities should not be mixed and it is not possible to consider the uncertainties as including the inaccuracies.

4.3 Impact of a Calibration Shot

To minimize the location inaccuracies, calibration shots may be used in wells. This is routinely performed for enhanced oil and gas recovery during hydraulic fracturing operations (e.g. Bardainne and Gaucher 2010). Although the temperature conditions may be different in geothermal wells, downhole explosions or alternative solutions (e.g. reverse VSP) could be considered. Here, we investigate the effects such a calibration shot could have in the earthquake location problem at Rittershoffen. Thus, we assume that a shot has been performed in the GRT1 well at the mid-depth of the open-hole section and that it was perfectly recorded by all stations of the three networks. Then, we calculate the travel time, in the 3D fault model (the true Earth), of the P- and S-waves to every station to generate the observations. The time differences of these arrivals with the theoretical arrivals computed in the assumed 1D velocity model (used for relocation) will be applied as station corrections. Such a station correction could be calculated in reality.

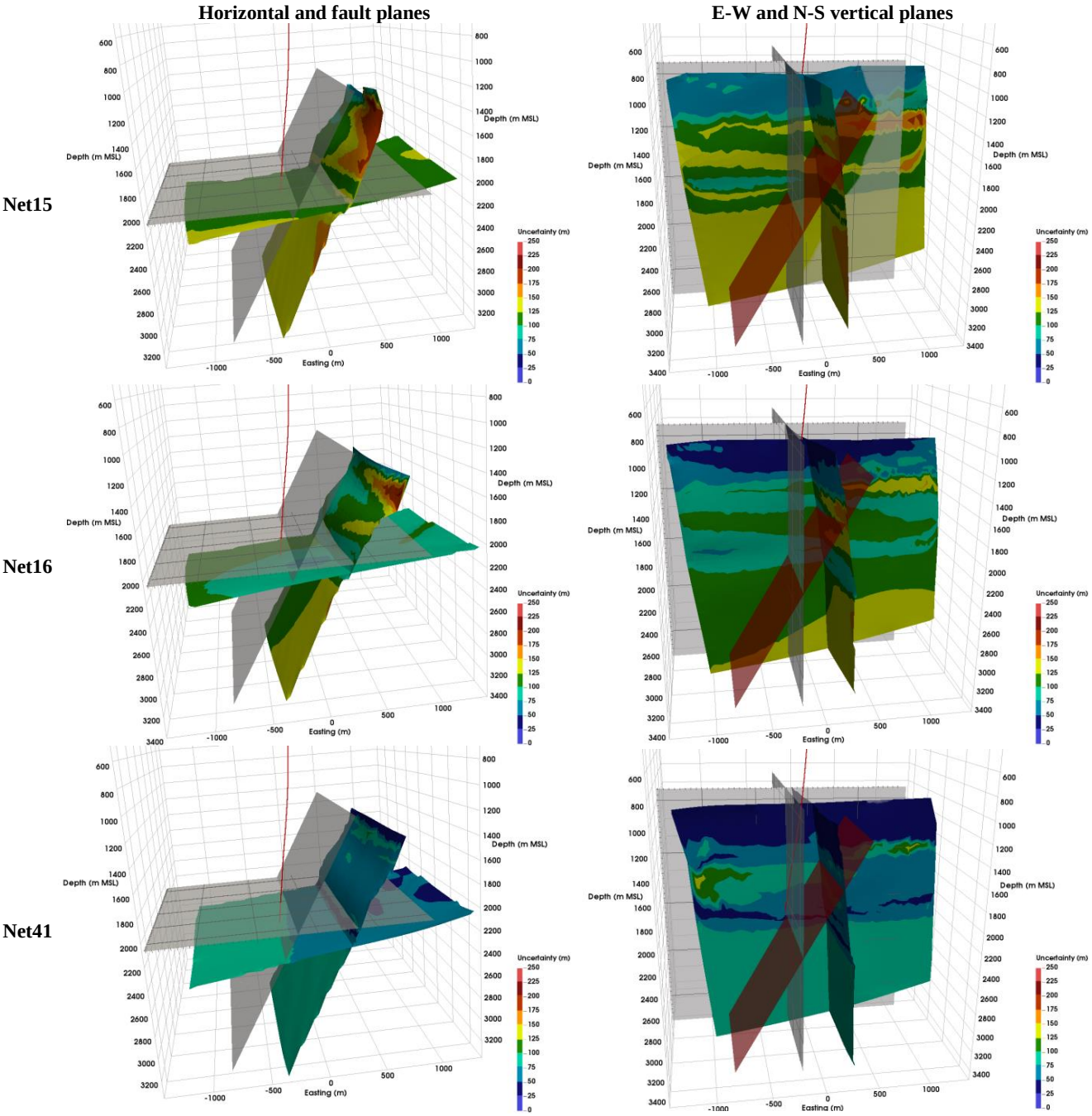

Figure 5: 3D view of the relocation of the synthetic events initially located on the horizontal plane and along the fault (left column) and on the N-S and E-W vertical planes (right column), for the Net15 (top row), Net16 (middle row) and Net41 (bottom row) networks. The initial locations are on the grey planes whereas the relocations are on the colored surfaces. The color scale is associated with the uncertainty which ranges between 0 m and 250 m. The GRT1 well trajectory is shown (red line).

Like Figure 5, Figure 6 shows, for the three networks, the four initial earthquake planes and the corresponding four surfaces on which the earthquakes are relocated, but after application of the station corrections.

One can first see a clear improvement of the relocations: for the three seismic networks, the location inaccuracies are strongly decreased by applying the station corrections. The earthquakes are no longer systematically shifted eastward from their initial position. The initial source planes become much less curved after relocation. All other effects on the source planes which have been noticed previously (dipping, rotating, bending) either disappear or become negligible.

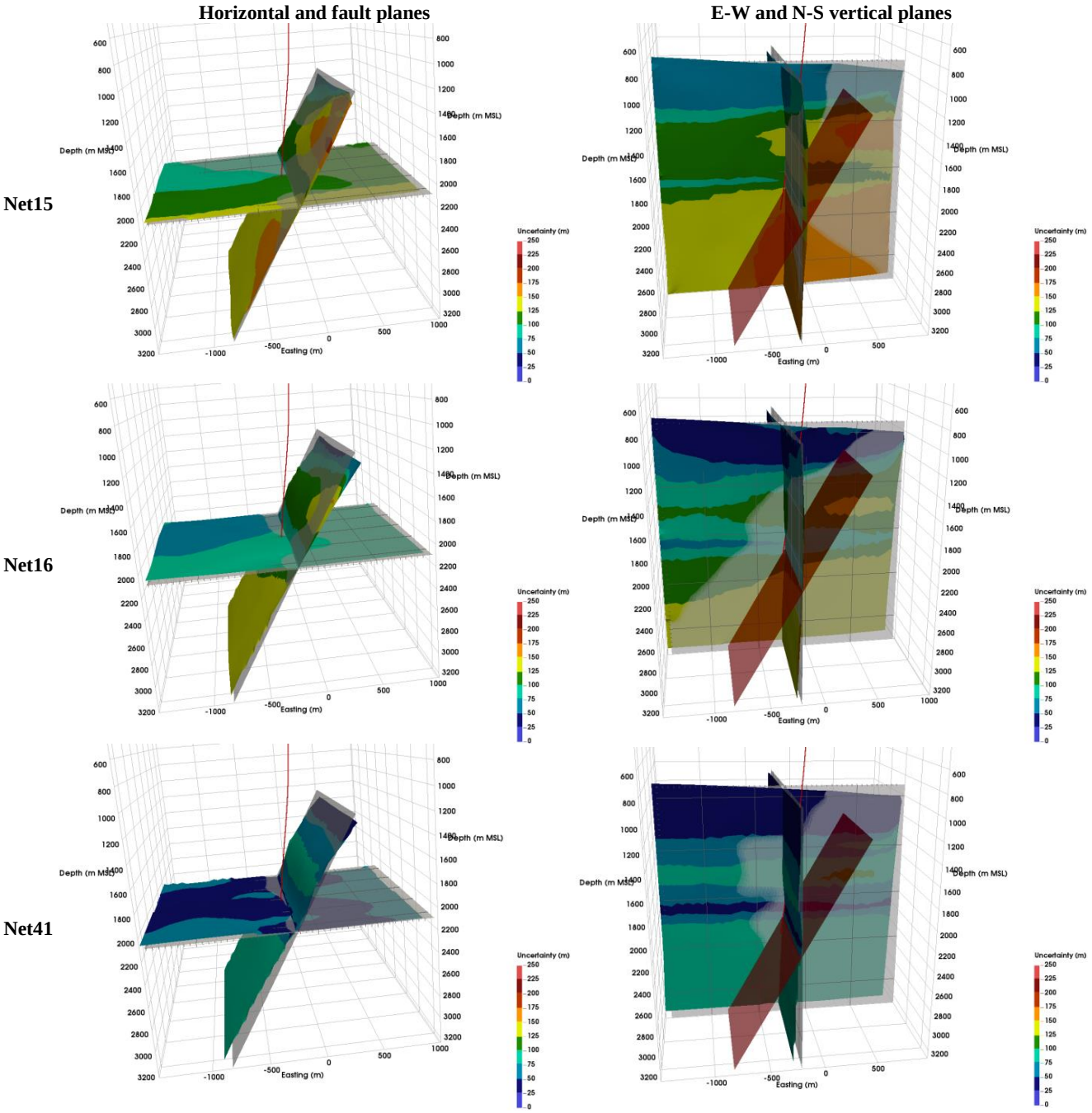

Figure 6: Same as Figure 5 but after application of the station corrections.

Along the fault, the median of the horizontal inaccuracy now ranges between 20 and 55 m with Net15, 18 and 46 m with Net16 and 18 and 58 m with Net41. With the last two networks, however, the shift is either eastward (for the shallowest sources) or westward (for the deepest sources). The vertical inaccuracy also changes and the shallowest sources are relocated deeper whereas the deepest sources are relocated shallower, thus squeezing the plane vertically. This effect is also visible on the E-W plane where the vertical inaccuracy increases with longitude. Still for this E-W plane, the inaccuracy median with depth ranges between 30 and -50 m with Net15, 20 and -80 m with Net16 and 30 and -100 m with Net41. The median of the horizontal inaccuracy measured on the horizontal plane is now ranging from west to east between 25 and 100 m with Net15, 35 and 80 m with Net16 and 20 and 90 m with Net41.

With regards to the interpretation of planar features delineated by earthquake hypocenters, the locations obtained after application of the station corrections do not strongly distort nor shift the original features. Nonetheless, the depth of the earthquake is the most affected parameter, and this has the tendency to make planes dipping more to the East.

Although the effect is quantitatively smaller, like in the uncalibrated case and for the same reason, the addition of one or more stations to the smallest network Net15 does not improve the location accuracy, on the contrary. The calibration shot allows correcting seismic travel times for one specific point underground but does not correct for the seismic ray path discrepancies between the 3D fault model and the 1D model.

As also shown on Figure 6, the location uncertainties are of the same order as previously seen. It looks like the station correction application smoothes the uncertainty variations on the considered planes. Additionally, the depth distribution of the uncertainties becomes very similar to the unperturbed velocity case without major differences between the western and the eastern side of the fault.

After calibration, the location uncertainties and the inaccuracies are roughly of the same order of magnitude.

5. CONCLUSION

We have examined the propagation of velocity model errors in earthquake absolute locations. This has been applied to the Rittershoffen geothermal field. Hence, we investigated the volume in which seismicity was already induced: between 1.5 and 4.5 km depth, 1.5 km around the well GRT1, and we used three seismic network lay-outs encountered during the monitoring of the area. Because both wells of the geothermal doublet are targeting a N-S 60° dipping normal fault, it was decided to use a 3D model including the fault and its associated vertical shift to represent the true Earth. However, as it is often done even at this reservoir scale, we took a 1D velocity model to relocate the seismicity in order to quantify the effects in the earthquake hypocenter locations.

The results show that large location bias is induced by neglecting the fault and the associated shifted blocks at Rittershoffen. This effect gets worst when the seismic network becomes denser and better covers the area. This is due to the addition of inconsistent observations (between the real Earth and its model) into the inverse location problem. Hypocenter shifts of the order of 350 m could be measured for the network located in the north-western part of the area (Net15), but shifts of the order of 450 m were seen for the dense and homogeneous network around the area (Net41). These inaccuracies represent 14 to 18% of the event depth. The results also highlighted that the inaccuracies are neither constant in direction nor in amplitude but depend on the event location, the velocity model and the seismic network. This prevents from applying a systematic and constant correction factor to the relocated hypocenters. Besides, original planar features delineated by event distributions are generally translated, distorted, rotated, squeezed or stretched. Since their geometrical characteristics are not preserved, direct interpretation of seismicity alignments in terms of location, azimuth and dip of major structures would be misleading.

Contrarily to the inaccuracies, the location uncertainties decreased with the increasing number of seismic stations in the network. Hence, the amplitude difference between both quantities increases with the number of stations. This stresses that the two quantities have very different origins and meanings, and should not be confused. The computed uncertainties were generally smaller than the corresponding inaccuracies accordingly, the latter could not be considered as included in the former.

To correct from the location bias, we simulated a calibration shot in the GRT1 well. The known position of this shot allowed us applying station corrections to remove time delays between the seismic propagation times in the 3D fault model and in the 1D velocity model. This procedure enabled to strongly decrease the hypocenter location bias, the depth inaccuracies being however less affected. Consequently, the planar features delineated by seismicity are almost not changed anymore.

Common sense recommends using any *a priori* information to better constrain the initial velocity model; this is confirmed by the present study. However, in the absence of information, we also showed the value added by performing a calibration shot in the well, close to the source location: the earthquake location accuracy can strongly increase which is beneficial for interpreting correctly geometrical features highlighted by the seismicity.

For Rittershoffen, the quantitative results of this study can constitute an *a priori* knowledge useful for interpretation or processing of seismological data. To some extent, they can be used in existing or future geothermal fields developed in similar geological settings. Since the described methodology is independent from the induced seismicity recorded at the site, it can also help to quantify the location capabilities of a given network at a given site, even prior to the network deployment.

ACKNOWLEDGMENTS

This work was conducted in the frame of the excellence laboratory “Labex G-EAU-THERMIE PROFONDE” (University of Strasbourg). It was partly funded by the “Investments for the future” program of the French National Research Agency, by the Energie Baden-Württemberg AG (EnBW), and by the French-German University (DFH-UFA). We wish to thank the ECOGI joint venture and the Électricité de Strasbourg – Géothermie company (ESG) for sharing data. We are grateful to V. Maurer, A. Genter, C. Baujard (ESG) and J. Schmittbuhl (CNRS – University of Strasbourg) for numerous discussions about this work and to N. Cuenot (EEIG “Heat Mining”) for sharing his experience on the Rittershoffen raw seismic data.

REFERENCES

Baillieux P., Schill E., Edel J.-B. and Mauri G. 2013. Localization of temperature anomalies in the Upper Rhine Graben: insights from geophysics and neotectonic activity. *International Geology Review* **55** (14), 1744–1762.

Bardainne T. and Gaucher E. 2010. Constrained tomography of realistic velocity models in microseismic monitoring using calibration shots. *Geophysical Prospecting* **58** (5), 739–753.

Baujard C., Genter A., Maurer V., Dalmais E., Graff J.-J. and Schmittbuhl J. 2014. The ECOGI EGS project in Rittershoffen, France. In: *Geothermal Resources Council Annual Meeting*, Geothermal Resources Council Annual Meeting, Portland, OR, USA. Geothermal Resources Council. ISBN 9780934412995.

Cornet F.H., Bérard T. and Bourouis S. 2007. How close to failure is a granite rock mass at a 5 km depth? *International Journal of Rock Mechanics and Mining Sciences* **44** (1), 47–66.

Edwards B., Kraft T., Cauzzi C., Kästli P. and Wiemer S. 2015. Seismic monitoring and analysis of deep geothermal projects in St Gallen and Basel, Switzerland. *Geophysical Journal International* **201** (2), 1022–1039.

Frietsch M., Groos J. and Ritter J.R. 2015. Detection and Delineation of a Fracture Zone with Observation of Seismic Shear Wave Anisotropy in the Upper Rhine Graben, SW Germany. *Pure and Applied Geophysics* **172** (2), 267–282.

Gaucher E., Maurer V., Wodling H. and Grunberg M. 2013. Towards a dense passive seismic network over Rittershoffen geothermal field. In: *European Geothermal Workshop 2nd*, Strasbourg, France.

Gaucher E., Schoenball M., Heidbach O., Zang A., Fokker P.A., van Wees J.-D. and Kohl T. 2015a. Induced seismicity in geothermal reservoirs: A review of forecasting approaches. *Renewable and Sustainable Energy Reviews* **52**, 1473–1490.

Gaucher E., Schoenball M., Heidbach O., Zang A., Fokker P.A., van Wees J.-D. and Kohl T. 2015b. Induced seismicity in geothermal reservoirs: Physical processes and key parameters. In: *World Geothermal Congress 2015*, World Geothermal Congress, Melbourne, Australia.

Genter A. 1989. *Géothermie Roches Chaudes Sèches: le granite de Soultz-sous-Forêts (Bas-Rhin, France)*.

Gesret A., Desassis N., Noble M., Romary T. and Maisons C. 2015. Propagation of the velocity model uncertainties to the seismic event location. *Geophysical Journal International* **200** (1), 52–66.

Held S., Genter A., Kohl T., Kölbel T., Sausse J. and Schoenball M. 2014. Economic evaluation of geothermal reservoir performance through modeling the complexity of the operating EGS in Soultz-sous-Forêts. *Geothermics* **51** (0), 270–280.

Husen S., Kissling E. and Deschwanden A. 2013. Induced seismicity during the construction of the Gotthard Base Tunnel, Switzerland: hypocenter locations and source dimensions. *Journal of Seismology* **17** (1), 63–81.

Kinnaert X., Gaucher E., Achauer U. and Kohl T. in revision. Modelling earthquake location errors at a reservoir scale: a case study in the Upper Rhine Graben. *Geophysical Journal International*.

Kraft T. and Deichmann N. 2014. High-precision relocation and focal mechanism of the injection-induced seismicity at the Basel EGS. *Geothermics* **52** (0), 59–73.

Lengliné O., Lamourette L., Vivin L., Cuenot N. and Schmittbuhl J. 2014. Fluid-induced earthquakes with variable stress drop. *Journal of Geophysical Research: Solid Earth* **119** (12), 8900–8913.

Lomax A., Virieux J., Volant P. and Berge-Thierry C. 2000. Probabilistic Earthquake Location in 3D and Layered Models. In: *Advances in Seismic Event Location*, Vol. 18 (ed. C. Thurber and N. Rabinowitz), pp. 101–134. Springer Netherlands. ISBN 978-90-481-5498-2.

Maurer V., Cuenot N., Gaucher E., Grunberg M., Vergne J., Wodling H., Lehujeur M. and Schmittbuhl J. 2015. Seismic monitoring of the Rittershoffen EGS project (Alsace, France). In: *World Geothermal Congress 2015*, World Geothermal Congress, Melbourne, Australia.

Meixner J., Schill E., Grimmer J.C., Gaucher E., Kohl T. and Klingler P. 2016. Structural control of geothermal reservoirs in extensional tectonic settings: An example from the Upper Rhine Graben. *Journal of Structural Geology* **82**, 1–15.

Pavlis G.L. 1986. Appraising earthquake hypocenter location errors: A complete, practical approach for single-event locations. *Bulletin of the Seismological Society of America* **76** (6), 1699–1717.

Podvin P. and Lecomte I. 1991. Finite difference computation of traveltimes in very contrasted velocity models: a massively parallel approach and its associated tools. *Geophysical Journal International* **105** (1), 271–284.

Sausse J., Dezayes C., Dorbath L., Genter A. and Place J. 2010. 3D model of fracture zones at Soultz-sous-Forêts based on geological data, image logs, induced microseismicity and vertical seismic profiles. *Comptes Rendus Geoscience* **342** (7-8), 531–545.

Tarantola A. 2005. *Inverse problem theory and methods for model parameter estimation.* Society for Industrial and Applied Mathematics.

Tarantola A. and Valette B. 1982. Inverse problems = quest for information. *Journal of Geophysics* **50**, 159–170.

Wittlinger G., Herquel G. and Nakache T. 1993. Earthquake location in strongly heterogeneous media. *Geophysical Journal International* **115** (3), 759–777.

Zang A., Oye V., Jousset P., Deichmann N., Gritto R., McGarr A., Majer E. and Bruhn D. 2014. Analysis of induced seismicity in geothermal reservoirs – An overview. *Geothermics* **52** (0), 6–21.